

# The modelling of the action potentials in myelinated nerve fibres

Kert Tamm<sup>[a]</sup>, Tanel Peets<sup>[b]</sup> and Jüri Engelbrecht<sup>[c]</sup>

[a] kert.tamm@taltech.ee, Tallinn University of Technology, Department of Cybernetics

[b] tanel.peets@taltech.ee, Tallinn University of Technology, Department of Cybernetics

[c] je@ioc.ee, Tallinn University of Technology, Department of Cybernetics and Estonian Academy of Sciences

## Abstract

The classical Hodgkin-Huxley model describes the propagation of an axon potential (AP) in unmyelinated axons. In many cases the axons have a myelin sheath and the experimental studies have then revealed significant changes in the velocity of APs. In this paper, a theoretical model is proposed describing the AP propagation in myelinated axons. As far as the velocity of an AP is affected, the basis of the model is taken after Lieberstein, who included the possible effect of inductance that might influence velocity, into the governing equation. The proposed model includes the structural properties of the myelin sheath: the  $\mu$ -factor (the ratio of the length of the myelin sheath and the Ranvier node) and g-ratio (the ratio of the inner-to-outer diameter of a myelinated axon) through parameter  $\gamma$ . It is demonstrated that the Lieberstein model can describe all the essential effects characteristic to the formation and propagation of an AP in an unmyelinated axon. Then a phenomenological model for a myelinated axon is described including the influence of the structural properties of the myelin sheath and the radius of an axon. The numerical simulation using the physical variables demonstrates the changes in the velocity of an AP as well as the changes in its profile. These results match well the known effects from experimental studies.

**Keywords:** action potential, nerve fibre, myelinated axon, velocity, mathematical modelling

## 1 Introduction

The celebrated Hodgkin-Huxley (HH) model can describe the action potential (AP) in an unmyelinated axon taking into account sodium and potassium ion currents [19]. The strength of the HH model is in the detailed description of the physics of ion currents but the cable equation describing the propagation of an AP is simplified by neglecting the inductance. There are several ways to improve this classical model towards a better description of the structural properties of axons and taking into account the accompanying effects. Many studies are devoted to the description of mechanical and/or thermal effects accompanying the propagation of an AP [5, 8, 10, 23] resulting in the formation of an ensemble of waves. These theoretical models are based on experimental results [22, 38, 39, 41, 42, 46]. Another important avenue of studies is related to modelling the behaviour of an AP in myelinated axons. An unmyelinated axon can be modelled like a cylindrical tube with a wall made of a biomembrane composed of a lipid bilayer. In the case of the myelinated axon, this bilayer has a myelin sheath which consists of multiple layers of a glial membrane composed of lipids and proteins and serves as an insulator [6, 43] or in some scenarios even as signal modulating element [12]. It means that under the myelin sheath the ion currents through the basic biomembrane proposed by Hodgkin and Huxley [19], do not exist. However, the myelin sheath is interrupted by Ranvier nodes where the usual HH model works. It is proposed that under the myelin sheath, the passive cable equation (the diffusion-type equation) governs the process and in Ranvier nodes, the usual HH equation works [13, 16]. However, it is demonstrated experimentally that under the myelin sheath, the velocity of the AP is increasing. This effect was already reported by Lillie in 1924 [26] and is nowadays referred to as the Lillie transition [47] or saltatory conduction (see [21]).

In this paper, a phenomenological model is proposed for describing the propagation of an AP in a myelinated axon. The most important question is how to model the possible changes in the propagation velocity of an AP due to the myelin sheath. The process is nonlinear and we follow a recommendation of Whitham [45]: “... one should not always turn too quickly to a search for the  $\epsilon$ .” In the context of the governing equation, it means that we should keep the neglected inductance. This idea is supported by Wang et al [44] who have argued that inductance is “a missing piece of neuroscience”. If we keep the inductance in the cable equation then under the myelin sheath the propagation is governed not by a diffusion (see [16]) equation but by a

hyperbolic equation. This hypothesis may better explain the changes in the velocity of an AP. Once the experimental studies have revealed the dependence of the velocity on the diameter of a fibre then such a dependence should also be taken into account.

In what follows, the model of Lieberstein [25] is a basic one to describe the AP propagation in myelinated axons. This model includes the HH ion currents but in addition, includes the inductance as it follows from the Maxwell equations. For proper modelling of the processes in myelinated axons, the influence of the myelin sheath must certainly be taken into account. In principle, the length of a myelinated section and its thickness are the leading structural factors in the process. Consequently, one important parameter is the ratio of lengths of a Node of Ranvier  $L_1$  and a myelinated section  $L_2$  in the form of the myelin length ratio (or the  $\mu$ -ratio for short) which is proportional to  $L_2/L_1$ . Another important parameter is the g-ratio (see [32]) which is the ratio of the inner-to-outer diameter of a myelinated axon. These parameters take into account the structure of a myelin sheath (cf analysis by Bassler [3]).

Section 2 is devoted to the analysis of the Lieberstein [25] model for the unmyelinated axon. The profiles of an AP found by the numerical simulation using the physical units [19, 25] demonstrate the accuracy of the model. The results confirm the earlier analysis by Kaplan and Trujillo [24] but more details are given. The profiles of ion currents and phenomenological variables  $n$ ,  $m$ , and  $h$  are also presented. It is shown that the head-on-collision of two APs leads to annihilation. The influence of the refraction length for the formation of consecutive APs is also analysed as well as the dependence of the velocity on the diameter of the axon. This forms a solid basis for the modelling of the APs in myelinated axons. Section 3 describes experimental results on myelinated axons focused on velocity changes [2, 27, 34], This analysis permits us to propose in Section 4 a phenomenological model describing the propagation of an AP in a myelinated axon influenced strongly by the structure of a myelin sheath ( $\mu$ -ratio). The structure of the governing equations follows the Lieberstein model (see Section 2) where the inductance leads to a wave-like behaviour but the final velocity of an AP depends on ion currents. The numerical simulations demonstrate clearly the changes in the velocity under the myelin sheath as well as the changes in the profile of the propagating AP. Finally, in Section 5 the discussion is presented with conclusions. As far as the numerical simulations are carried on with physical variables, the results could be better checked in experimental studies.

## 2 Lieberstein model for AP propagation on unmyelinated axon

Experimental studies of processes in the myelinated axons have demonstrated that the signal propagates faster than in unmyelinated axons [1, 14]. Although there are several plausible explanations for this phenomenon, there is no clear consensus in the scientific community about the exact physical background of this effect. Consequently, in deriving a mathematical model, all possible phenomena that could influence the propagation velocity should be taken into account, even if some of these could be considered much smaller than others at first glance (see, for example, the book by Whitham [45]).

### 2.1 Basic model

The cable equation used by Hodgkin and Huxley [19] for deriving the model for the electrical signal propagation is parabolic, i.e., inductance is neglected. Indeed, its influence is small but following Whitham [45] we use here the full model of Lieberstein [25] derived directly from Maxwell equations [28]. This model is hyperbolic but the final velocity of the signal is influenced by ion currents like in the HH model [19].

Here we go briefly over the key points from [25] and add some comments to make it easier to follow later in the paper what and why is changed when including the effects of myelination in the next Section.

Lieberstein [25] starts with an elementary form of Maxwell equations for current and voltage on a long line

$$\frac{\partial i_a}{\partial x} + i + \pi a^2 C_a \frac{\partial V}{\partial t} = 0, \quad (1)$$

$$\frac{\partial V}{\partial x} + r i_a + \frac{L}{\pi a^2} \frac{\partial i_a}{\partial t} = 0, \quad (2)$$

where

- $x$  is space (length) and  $t$  is time;
- $V$  is the action potential,  $i_a$  is the axon current per unit length (along the axon) and  $i$  is the membrane current per unit length (taken the same as HH current across the membrane later in the paper);
- $a$  is the radius of the axon,  $r$  is the axon resistance per unit length,  $L$  is the axon specific self-inductance and  $C_a$  is the axon self capacitance per unit area per unit length.

It is noted that the membrane current density (which is what is used in the HH model [19]) is

$$I = \frac{i}{2\pi a}, \quad (3)$$

and the specific resistance of the axon is

$$R = \pi a^2 r. \quad (4)$$

The structure and the physical interpretation of the governing equations (1) and (2) is easier to see if writing it as a single second-order PDE (see eq. (3) in [25]):

$$\frac{\partial^2 V}{\partial x^2} - LC_a \frac{\partial^2 V}{\partial t^2} = RC_a \frac{\partial V}{\partial t} + \frac{2}{a} RI + \frac{2}{a} L \frac{\partial I}{\partial t}, \quad (5)$$

where on the left-hand side (LHS) there is a classical wave equation type operator while on the right-hand side (RHS) there are dissipation-type elements (first order partial time derivatives) which either remove energy from the system or add it to the system depending on the sign. In the context of signal propagation in nerve fibres, the ionic currents across the membrane change the membrane potential in a given location while some of that energy is lost during the diffusion-type propagation along the axon to the axon resistance. At the same time, the LHS operator ensures that part of the signal is propagating like a classical wave.

Returning to the system as two coupled eqs. (1) and (2) the membrane current  $I$  is taken (this is what is different from regular Telegrapher's equation) as it was proposed in the HH model [19] as

$$I = C_m \frac{\partial V}{\partial t} + I_{Na} + I_K + I_l, \quad (6)$$

where  $I$  is the total membrane current density (positive direction is into the axon),  $V$  is the membrane potential relative to the resting potential (depolarisation is negative),  $C_m$  is the membrane capacity per unit area while  $I_{Na}$  and  $I_K$  are currents which are defined through "equilibrium potentials" for Na and K ions while  $I_l$  is "leakage current" representing *all* other ionic currents (Hodgkin and Huxley point mostly at chlorine Cl, however, Ca is also potentially relevant which some authors claim to be about as important as Na and K ions) and is chosen so that at resting potential leakage current across the membrane would be zero.

In eq. (1) we have  $i$ , so  $i = I2\pi a$  and if one takes  $I$  as expressed in eq. (6) inserting it into eq. (1), we can get expression

$$C_a \pi a^2 \frac{\partial V}{\partial t} + \frac{\partial i_a}{\partial x} + 2\pi a \left( C_m \frac{\partial V}{\partial t} + I_{Na} + I_K + I_l \right) = 0. \quad (7)$$

Further, changing notation from  $V \rightarrow Z$ , inserting  $I_{Na}, I_K, I_l$  [19] and collecting both time derivatives in eq. (7), we get:

$$(C_a \pi a^2 + C_m 2\pi a) \frac{\partial Z}{\partial t} + \frac{\partial i_a}{\partial x} + 2\pi a \cdot [g_{\hat{K}} n^4 (Z - Z_K) + g_{\hat{Na}} m^3 h (Z - Z_{Na}) + \hat{g}_l (Z - Z_l)] = 0, \quad (8)$$

and from eq. (2):

$$\frac{L}{\pi a^2} \frac{\partial i_a}{\partial t} + \frac{\partial Z}{\partial x} + r i_a = 0. \quad (9)$$

Equations (8) and (9) can be solved numerically with the pseudospectral method.

The dimensions of coefficients in eqs. (8) and (9) are:  $C_a \left[ \frac{F}{m^3} \right]$ ,  $C_m \left[ \frac{F}{m^2} \right]$ ,  $a[m]$ ,  $n, m, h$  are dimensionless,  $g_{\hat{K}}, g_{Na}, \hat{g}_l \left[ \frac{S}{m^2} \right]$  ( $S$  denotes SI-unit siemens) while the membrane potential  $Z[V]$  and current  $i_a[A]$ .

What does it mean to keep the inductance  $L$  contrary to the celebrated classical HH model [19]? One possible way of making sense of the differences is by looking at the equations. In the case of the system of

PDEs (eqs. (1) and (2) in [25]), it can be seen that there is a term  $\partial i_a / \partial t$  in eq. (2). This can be interpreted as the rate of change of current along an axon. In the HH model, the axon current is “hidden” in term  $\partial^2 V / \partial x^2$ . Another possibility is to look at the Lieberstein model in the form of one PDE (eqs. (3) and (6) in [25]). It can be seen in eq. (3) that two additional terms appear in the Lieberstein model compared to the classical HH model  $-\partial^2 V / \partial t^2$  and  $\partial I / \partial t$ . The second partial derivative is what makes the model hyperbolic and as pointed out by Kaplan and Trujillo [24], it influences the maximum velocity of the AP. However, the term  $\partial I / \partial t$  is an even more notable difference as the time derivative of the ion current is not present in the classical HH model. In eq. 6 in [24] it can be seen that inductance affects the ion currents and also time derivatives of gating variables  $n, m, h$  arise. One should note that Kaplan and Trujillo [24] have calculated axon inductance from the movement of ions as  $4421 [mH \cdot cm]$  if AP velocity is  $12.3 [m/s]$  at  $a = 238 [\mu m]$ .

## 2.2 Moving frame of reference and inductivity

Lieberstein [25] assumes that accounting for the inductivity (unlike in the HH model where it was neglected) he can go into a moving frame of reference in a standard way introducing  $\xi = x - \Theta t$ . However, we should note that it could be, actually  $\xi = x \pm \Theta t$ , where  $\Theta$  is velocity, as taking only a single direction means discarding the wave propagating in the opposite direction. It should be noted that using a moving frame of reference allows one to also derive an evolution equation (a single wave) for the nerve pulse [9]. Lieberstein [25] defined the velocity  $\Theta$  of the AP in an unmyelinated axon through axon radius, inductance and capacity as

$$\Theta = \sqrt{\frac{a}{2LC}}, \quad (10)$$

proceeding after that to writing up eqs (1) and (2) in the moving frame of reference. For the sake of completeness, it should be noted that in (10) Lieberstein [25] argued that for capacitance  $C$  the axon self-capacitance  $C_a$  contribution can be neglected because  $C = \frac{a}{2}C_a + C_m$  and axon radius is small so the contribution of  $C_a$  is small compared to membrane capacity per unit area  $C_m$ .

More recently, Fukasawa and Takizawa [15] have also investigated the question of electrical signal propagation velocity in an axon if inductivity is taken into account including the question of how to estimate the inductance parameter value.

In the present paper, we have opted to avoid going into a moving frame of reference preferring to solve the model as a coupled pair of PDEs and to keep the influence of  $C_a$  for the sake of completeness, even if its influence on the behaviour of the solutions is arguably small.

## 2.3 Solutions of Lieberstein model

A numerical example (see Fig. 1) using pseudospectral method (see Appendix A in [10]) and periodic boundary conditions demonstrating the evolution of solutions for model equations (8) and (9) is now presented. The following parameters are used:  $n = 2^{11}$  (number of spatial nodes),  $t_{end} = 45$  (time in [ms]),  $C_m = 1 [\mu F/cm^2]$  (membrane capacitance),  $a = 1 [\mu m]$  (axon radius),  $R = 32 [m\Omega/cm]$  (axoplasm resistance) while the HH model parameters are the same as in [19] paper:  $G_{Na} = 120 [m\Omega/cm^2]$ ,  $G_K = 36 [m\Omega/cm^2]$ ,  $G_l = 0.3 [m\Omega/cm^2]$  and  $Z_{Na} = -115 [mV]$ ,  $Z_K = 12 [mV]$ ,  $Z_l = -10.613 [mV]$  while  $h_0 = 0.596$ ,  $n_0 = 0.318$ ,  $m_0 = 0.052$  (initial values for parameters  $h, n, m$  in HH model at  $t = 0$ ). We take in the following example the axoplasm capacitance as  $C_a = 0.1 [\mu F/cm^3]$  and  $r = R/(\pi a^2)$  (resistance of an axon per unit length) while the  $R$  is taken the same as in the classical paper by Hodgkin and Huxley [19]. We take  $L = 40 [mH \cdot cm]$  (inductivity) for the numerical example (resulting in  $1 [m/s]$  propagation velocity for the AP signal). We remark, that as noted earlier Kaplan and Trujillo [24], have calculated axon inductance from the movement of ions as  $4421 [mH \cdot cm]$  if AP velocity is  $12.3 [m/s]$  at  $a = 238 [\mu m]$ , however, as in our case the reference axon radius is taken smaller it makes sense to reduce the  $L$  value. Initially system is taken at rest and at  $t = 1 [ms]$  we generate a narrow bell-shaped pulse (“spark”) for the  $Z$  in the middle of the space domain which generates the propagating AP. In spatial units, the length of the computation node ( $\Delta n$  or  $\Delta x$ ) is  $61 [\mu m]$  while the total width of the computational domain in the space (from  $n = 1$  to  $n = 2048$ ) is  $4\pi [cm] \approx 12.56 [cm]$ .

It should be stressed, that the chosen parameters do not represent any particular model nerve as these have been collected from studies describing different experimental setups or even taken as a rough estimate (like

specific inductivity  $L$ ). Most of the parameters are taken from [19] corresponding to giant squid axon at about  $6.3[C^\circ]$  while inductivity  $L$  is chosen so that the AP signal would have propagation velocity of around  $1 [m/s]$  if the axon radius  $a$  is  $1 [\mu m]$ .

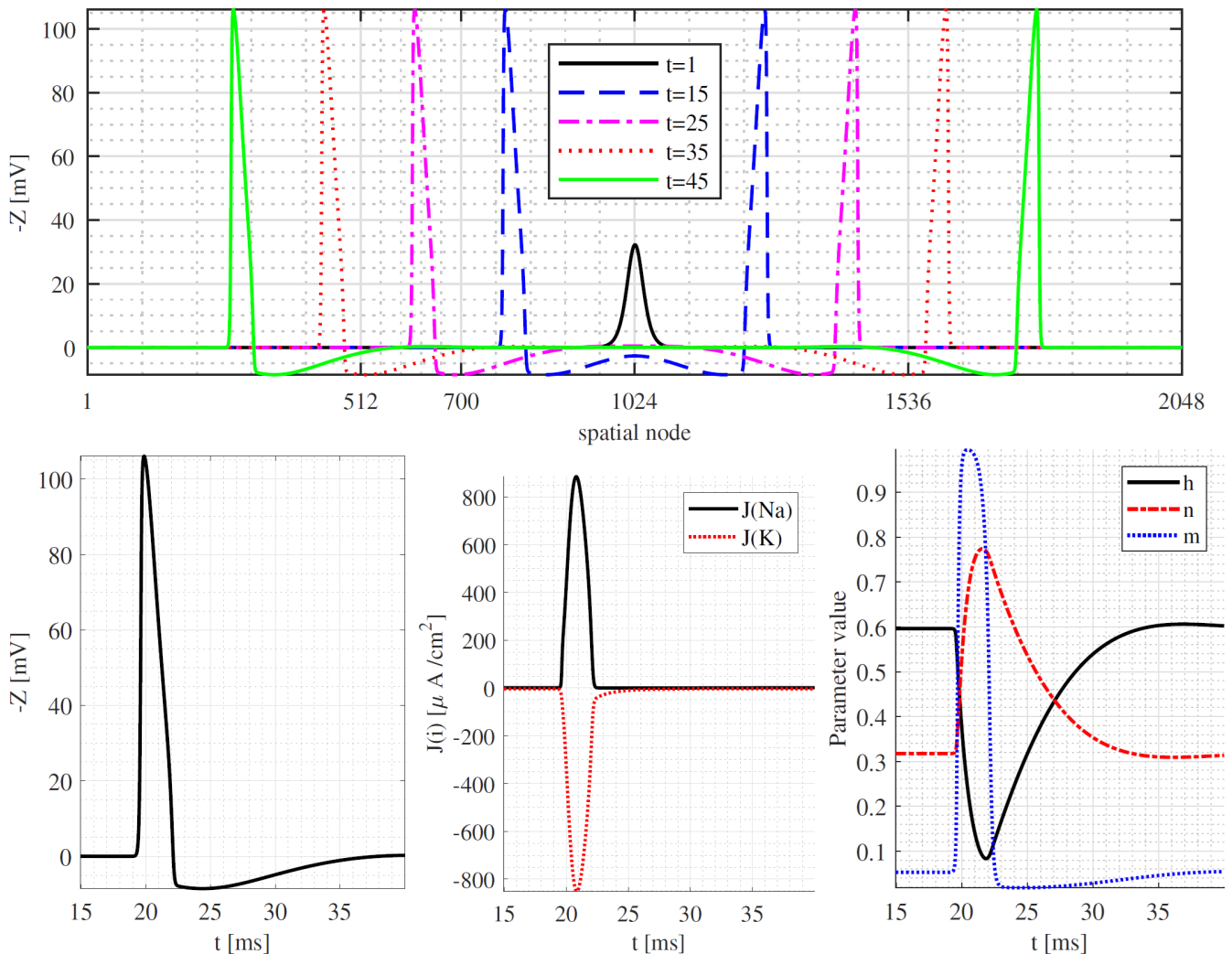


Figure 1: The top panel shows AP profiles in space from an initial “spark” centred at  $n=1024$  generated at  $t = 1$ . The bottom panels demonstrate the example solutions of eqs (8) and (9) in time at spatial node  $n = 700$ . The initial condition is zero, at  $t = 1$  ms a “spark”  $Z$  (narrow localised voltage pulse) is generated in space acting as initial excitation. It can be noted that the spark at 1 ms generates a propagating AP. The left panel shows the AP, the middle panel shows Na and K ionic currents and the right panel shows the changes of internal variables  $n, m, h$  in time.

In Fig. 1 it is demonstrated that the Lieberstein model has solutions which are characteristic of an AP in literature (for example, [19,25]), however, it is known that in physiology, an AP has a few more properties that must be fulfilled. These are: (1) electrical nerve signal must annihilate upon head-on collision, (2) a disturbance or signal generated during a short time after the signal has passed a location (so-called refractory period) must dissipate rapidly without generating a new AP (a minimum separation time before another nerve pulse can propagate). In Figs. 2 and 3 it is demonstrated that the Lieberstein model satisfies these conditions. As we are using periodic boundary conditions (nodes  $n = 1$  and  $n = 2048$  are connected so a wave hitting the boundary  $n = 2048$  enters the grid again from  $n = 1$ , as an example). Figure 2 demonstrates that during a head-on collision of propagating AP signals annihilate according to the Lieberstein model fulfilling the first condition for a realistic AP model. The left panel of Fig. 2 depicts the AP amplitude in time at boundary node  $n = 2048$  and the left panel depicts the spatial distribution of the signal when two spatial periods are plotted side by side (from 1 to  $2n$ ) making it clearer to see a head-on collision of propagating AP signals at the right boundary. The left panel of Fig. 3 demonstrates the emergence of the AP from the initial disturbance (centred at  $n = 1024$ ) above the threshold value given at  $t = 1$  and then  $10ms$  later another voltage spike is given at the same location at  $t = 11ms$  which dissipates rapidly. The middle panel

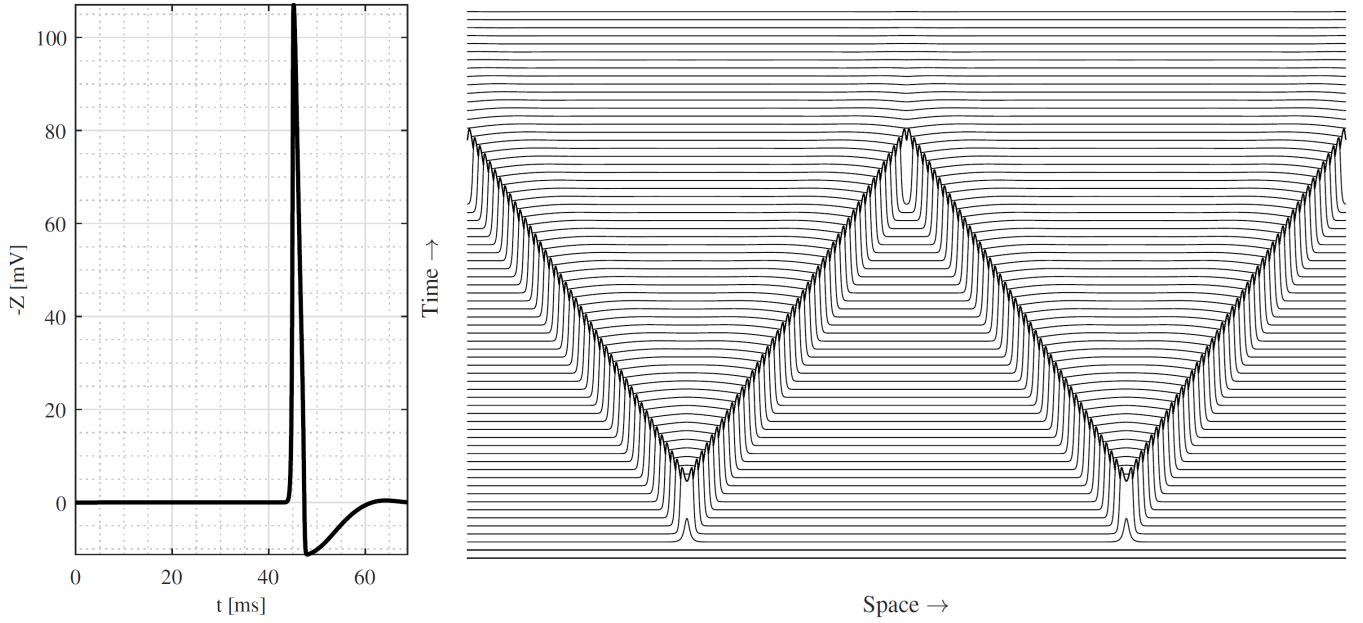


Figure 2: Example solutions of eqs (8) and (9). The initial condition is zero, at 1 ms a “spark” (narrow localised voltage pulse)  $Z$  is generated in space centered at  $n = 1024$  acting as initial excitation. The left panel shows the AP in time at  $n = 1$  (periodic boundary) demonstrating AP annihilation during a head-on collision, and the right panel shows the AP signal in space (two adjacent spatial grids plotted side by side,  $\Delta t = 1 [ms]$ ) demonstrating AP annihilation during a head-on collision at a boundary.

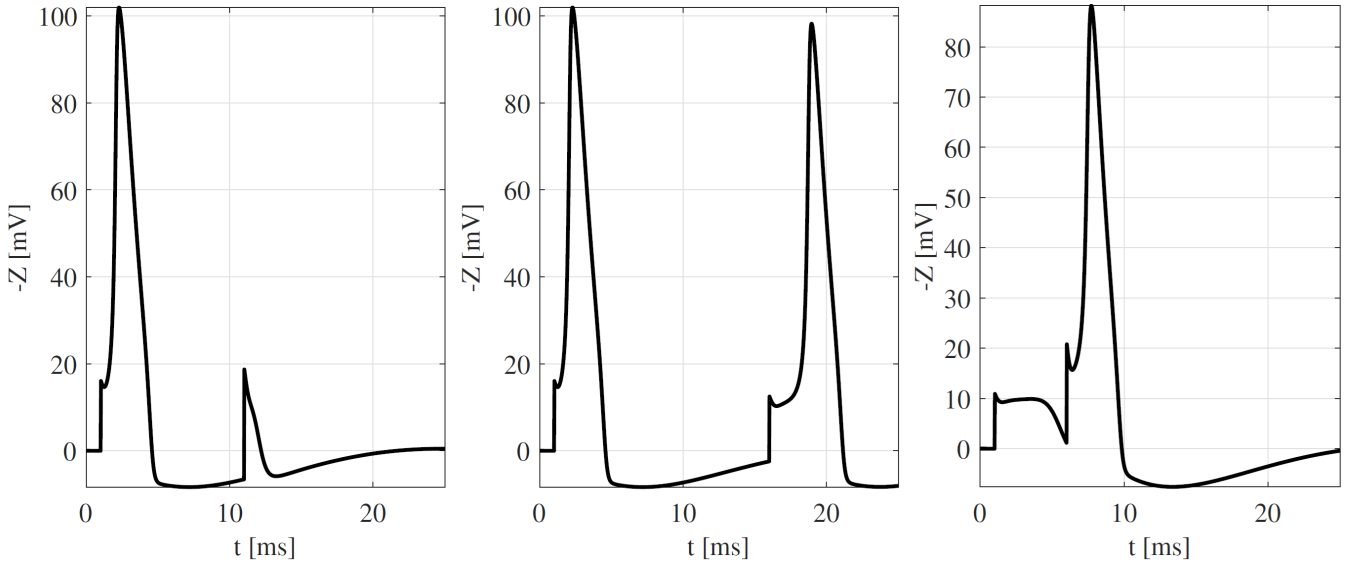


Figure 3: Example solutions demonstrating refractory period of eqs (8) and (9). The initial condition is zero, at 1 ms a “spark” (narrow localised voltage pulse)  $Z$  is generated in space centered at  $n = 1024$  acting as initial excitation. The left panel shows the AP in time at  $n = 1024$  and the second pulse is given at  $t = 11 [ms]$  which dissipates without generating the new AP, the middle panel shows a scenario where the second pulse is given at  $t = 16 [ms]$  which generates a new AP signal as  $15 [ms]$  is sufficient separation between the pulses at the chosen parameter values, the right panel shows a scenario where the first pulse at  $t = 1 [ms]$  is narrowly under the threshold value for generating a propagating AP, however, a secondary pulse is given at  $t = 6 [ms]$  before previous signal manages to fully dissipate pushing the signal above the threshold and generating a propagating AP signal.

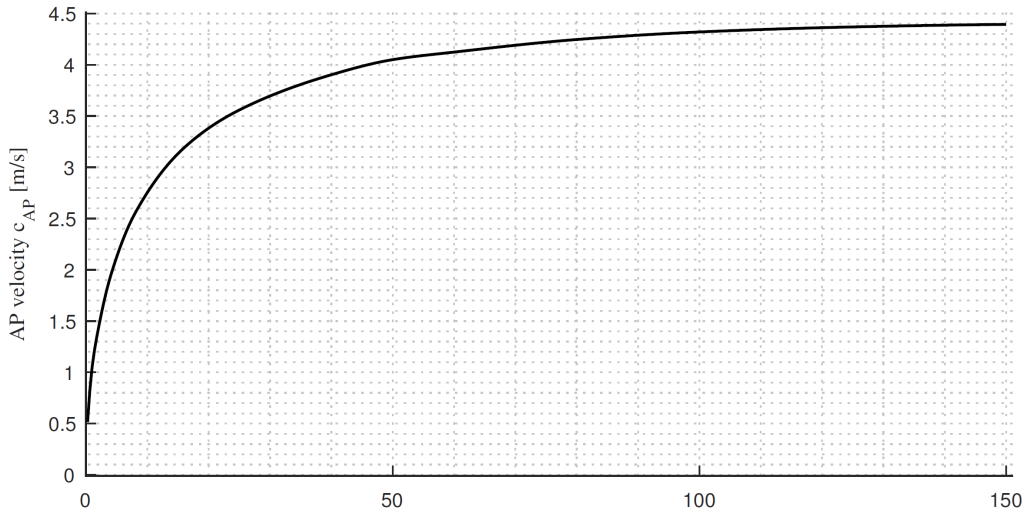


Table 1: AP velocity  $c_{AP}$  as a function of axon radius  $a$ .

$a$ [ $\mu m$ ]	0.25	0.50	1	2	4	8	16	25	40	50	60	80	100	125	150
$c_{AP}$ [ $m/s$ ]	0.5	0.75	1.0	1.4	1.95	2.55	3.2	3.55	3.9	4.0	4.1	4.25	4.3	4.35	4.4

Figure 4: The action potential propagation velocity as a function of the axon radius in the Lieberstein model. The table contains the calculated values of the AP velocity  $c_{AP}$ .

of Fig. 3 demonstrates that if a sufficient temporal separation between the pulses is given a repeating signal can be generated and the right panel of Fig. 3 shows a niche scenario where giving a small signal which is initially below the threshold value sufficiently frequently it is still possible to generate propagating AP if the combined dynamics succeeds in crossing the threshold value for the AP generation.

## 2.4 Influence of the axon radius on the propagation velocity of AP.

From earlier studies (see, for example, [29]) it is known that the propagation velocity of the AP is influenced by three factors – (i) space coefficient  $\lambda = \sqrt{R_m/R_a}$ , (ii) time coefficient  $\tau = R_m C_m$ , and (iii) the time measure  $T$  characterizing the time it takes to generate the AP on any point along the axon. The membrane resistance  $R_m$  scales inverse-proportionally with axon diameter  $R_m \propto 1/d$  while membrane capacitance  $C_m$  increases proportionally with axon diameter  $C_m \propto d$  while axial resistance  $R_a$  scales as  $R_a \propto 1/d^2$  meaning that the propagation velocity of AP is  $c_{AP} \propto \sqrt{d}$ .

We note that in the model parameters, the axon resistance is changed when the axon radius is changing so  $r = R/(\pi a^2)$ , where  $R$  is constant (as defined in the classical paper [19]). The propagation velocity of AP as a function of axon radius is depicted in Fig. 4 with the parameters used for a numerical example. It should be noted that the electrical circuit hypothesis for the AP propagation velocity (like  $c_{AP}^2 \propto a/(2R)$  for the HH model or  $c_{AP}^2 \propto a/(2LC)$  for the Lieberstein model) which is based on similarity with the chosen electrical circuit, while certainly useful, can overlook some potentially important mechanisms (like, for example, the influence of cytoskeleton) that are left aside during the many simplifications needed to get a simple electrical scheme. This means that in practical applications one has to consider carefully any conflicts between experimental observations and modelling results to determine if the model is sufficient for adequately describing the observed process. For example, while here we have chosen  $L$  so that at  $a = 1$  the AP velocity  $c_{AP}$  is  $\approx 1$  [ $m/s$ ] as a demonstration of the model behaviour, for practical applications that parameter would need to be determined from the electrophysiology of the problem under investigation as in reality, this is not a free parameter.

## 3 Description of a myelinated axon

The axon can be described as a tube filled with axoplasm and cytoskeleton with a lipid-bilayer (biomembrane) wall which is embedded in an intercellular medium (fluid) [6]. While some axons are unmyelinated, many of them have a myelin sheath (additional structure surrounding the axon formed by glial cells (oligodendrocytes

(in the central nervous system) or Schwann cells (in the peripheral nervous system)) that is in simplified terms composed of layers of biomembrane glued together with some proteins.

### 3.1 The structure of myelinated axon

The myelin sheath is interrupted by the nodes of Ranvier which play an important role in the nerve pulse propagation. A node of Ranvier is typically around 1  $\mu\text{m}$  in length and has a high density of ion channels [27] while myelin sheath segments are typically from roughly 50  $\mu\text{m}$  to 300  $\mu\text{m}$  in length. The distribution of the myelinated parts was once believed to be uniform, but now it is understood that the length of the myelinated parts and the nodes of Ranvier vary and unusually long nodes of Ranvier (50  $\mu\text{m}$ ) have been reported [43]. These long segments could play an important role in the synchronisation of nerve pulses by delaying an AP.

The myelin sheath is a stack of specialised plasma membrane sheets produced by glial cells that wrap around the axon [27]. A lipid bilayer (biomembrane) is typically from 3 to 4 nm in thickness and the main protein  $P_0$  (acting as a glue between lipid bi-layers) in the myelin sheath has about 4.5 nm central part and roughly similar size “tails” embedded in adjacent lipid bi-layers [31] that all together form a myelin sheath composed by many such layers surrounding the axon. The myelin sheath can be up to 2.5  $\mu\text{m}$  in thickness [17, 30, 33] and on the lowest theoretical limit, an extra layer of biomembrane surrounding the axon might be argued to be a myelin sheath. Typical axon diameter varies from about 0.5  $\mu\text{m}$  to 25  $\mu\text{m}$  [33] in mammals but can reach as high as about 1 mm in giant squids [20, 42]. For example, in peripheral nerve fibres the myelin sheath thickness starts from about 0.5  $\mu\text{m}$  for the smaller diameter axons and the upper value of 2.5  $\mu\text{m}$  is more characteristic to the axons with large diameter [33]. In peripheral nerves, myelin sheath thickness increases sharply, at first, when the axon radius increases from the smallest physiologically viable diameters and then the thickness increase gradually slows down as the axon diameter approaches the largest physiologically viable values [33] in these nerves.

Nodes of Ranvier contain much higher densities of various ion channels than elsewhere on axons. K and Ca channels are about 10 nm in length and roughly 4 nm in diameter [7]. Na channel is about 12 nm long and about 10 nm in diameter [35]. Structurally the myelinated part of the axon is divided into the following regions: next to the node of Ranvier is a region called the paranode. This is the area where the myelin attaches to the axon. The juxtaparanode is located next to the paranode and it is the area where most voltage-gated  $\text{K}^+$  ion channels are located. The  $\text{Na}^+$  channels are concentrated in the nodes of Ranvier. The geometry of a myelinated axon is sketched later in the paper in Fig. 5. The AP propagates down an axon without diminution at velocities up to 1 m/s (without myelin sheath) [27]. In non-myelinated neurons, the conduction velocity of an action potential is roughly proportional to the diameter of the axon [27]. The presence of a myelin sheath around an axon increases the velocity of impulse conduction to 10-100 m/s [27, 34].

### 3.2 Saltatory conduction mechanism hypothesis for myelinated axon

It is known that the myelination of the axon increases the propagation velocity of the AP and the prevalent explanation in the literature of this phenomenon is the saltatory conduction mechanism [4, 13]. As the capacity of the axon changes significantly between the myelinated and unmyelinated sections, this causes, in a nutshell, the electrical signal to “jump” between the nodes of Ranvier propagating faster than it would in the case of an unmyelinated axon. The saltatory conduction hypothesis is briefly summarized as follows.

In earlier studies, it is assumed that myelination increases effective membrane resistance (reduces permeability of ions) and decreases the capacitance of the membrane by several orders of magnitude. As noted, the propagation of AP along myelinated axons is considerably faster than in unmyelinated axons. In the context of the cable equation (which is a starting point for both HH and Lieberstein models) the usual explanation in literature is that transmembrane currents in the myelinated sections can be neglected meaning that the myelin sheath section can be taken in that case as a simple resistor (i.e, the sheath acts as an insulator). This phenomenon is called a saltatory (leaping) wave in earlier studies where AP is not propagating continuously along the axon but rather jumps from one node of Ranvier to another node of Ranvier [4].

In practice, the saltatory conduction hypothesis can be difficult to verify experimentally as measuring sharply localized AP (nodes of Ranvier are typically around 1  $\mu\text{m}$  long) is difficult. What is measured in classical experiments (for example, [14, 20, 22, 40]), is AP over some section of the axon (i.e, including the signal from both myelinated on non-myelinated sections, moreover most classical experiments are done



on non-myelinated axons). However, the proposed hypothesis appears to be a plausible (and popular in earlier studies) starting point to explain why the AP is faster in myelinated axons and we opt to use it as well. It should be noted that in effect we use interpretation which is partly inspired from the continuum mechanics [36] where we interpret the signal coming from the model not as the evolution of AP in time at a fixed point on axon as is typical but rather a combined signal one might get from a "unit cell" which contains a node of Ranvier and a myelinated section next to the node, based on assumption that characteristic wavelengths of the signal are much larger than the underlying scale of the micro-structure (nodes of Ranvier in  $\mu m$  range and myelinated sections typically in hundreds of  $\mu m$  in length [6, 27]). In comparison, the first harmonics (when looking at the Fourier spectrum of the signal) of the AP in space are from  $cm$  to tens of  $cm$  (depending on the duration and velocity of the signal) [11, 37].

Following [4], it is assumed that membrane potential is uniform within a given node of Ranvier (i.e, a node is an isopotential) and denoting the voltage of  $n$ th node as  $Z_n$  while treating the adjacent myelinated section as classical Ohmic resistor with resistance  $rL_m$  (where  $r$  is intracellular resistance per unit length and  $L_m$  is the length of myelinated section) the current  $I$  between nodes  $n$  and  $n + 1$  can be written as

$$I_{n+1} = -\frac{1}{rL_m} (Z_{n+1} - Z_n). \quad (11)$$

Considering the conservation of current at  $n$ th node implies that the total transmembrane current into that node can be written as

$$2\pi al \left( C_m \frac{\partial Z_n}{\partial t} + I_{ion} \right) = I_n - I_{n+1} = \frac{1}{rL_m} (Z_{n+1} - 2Z_n + Z_{n-1}), \quad (12)$$

where  $a$  is the radius of the axon. Bressloff [4] extracts term  $\partial Z_n / \partial t$  from (12) and constructs equation for the potential  $Z$  at node  $n$  as

$$\frac{\partial Z_n}{\partial t} = -\hat{I}_{ion} + D (Z_{n+1} - 2Z_n + Z_{n-1}), \quad (13)$$

where

$$D = \frac{R_m}{(2\pi ar) l L_m \tau_m} = \frac{\lambda_m^2}{l L_m \tau_m}. \quad (14)$$

Here  $R = \pi a^2 r$ ,  $\tau_m = R_m C_m$ ,  $\lambda_m = \sqrt{\frac{R_m a}{2R}}$  and  $l$  is the length of the node of Ranvier. The parameter  $D$  in (14) governs the saltatory conduction velocity between adjacent nodes of Ranvier under the simplifying assumptions done above and is a reasonable starting point. It is worth noting that the philosophy behind constructing eq. (13) is one of the typical approaches how the HH model (which in its ODE form describes signal evolution in time at a fixed spatial point on axon) is used to describe travelling AP signal – meaning that one constructs pseudo-numerical scheme where adjacent nodes interact and can propagate the signal that way along the axon.

We have to emphasize that in what follows, it is not the direct one-to-one adoption of the saltatory conduction mechanism as proposed in [4] as we are not only considering the electrical effects but also other influences from potentially relevant interactions (like cytoskeleton, for example) and as such, our approach is partly phenomenological. We opt to separate myelin geometry along the axon and perpendicular to the axon as theoretically easily observable and propose that the signal propagation velocity from node of Ranvier to node of Ranvier is governed by more than only membrane capacitor dynamics. This way, after the actual propagation velocity is determined from experimental observations, one can account for the influence of the membrane capacitor dynamics (which can be estimated from the myelination geometry and dielectric properties of the myelin) and then look into other potential influences, like fast enough chemical processes or interactions with the internal structures of the axon to quantify these and hopefully provide a more detailed insight towards functioning and signal propagation in an actual living nerve cell.

## 4 Model for AP propagation on myelinated axon based on Lieberstein model

Taking the elementary form of Maxwell equations combined with the ideas proposed by Lieberstein in eqs. (8) and (9) as a starting point, we proceed to modify these governing equations to include the effect of myelination on the AP signal propagation.

## 4.1 Hypotheses and governing equations

When we modify the Lieberstein model [25] to account for the effect of myelination on a nerve fibre, we consider the following hypotheses:

1. The velocity of the AP depends on the ratio of lengths between the myelin sheath and the node of Ranvier ( $L_2/L_1$ ) (so-called ‘ $\mu$ -ratio’ below);
2. The thickness of the myelin sheath affects the velocity of the AP signal (the so-called  $g$ -ratio) and could be taken into account indirectly through the capacitance variations (included in parameter  $\gamma$  below);
3. The dominant mechanism through which the AP signal velocity in myelinated nerve fibre is increased is the so-called saltatory conduction hypothesis [4];
4. The model equation should be reduced back to the basic model when the myelination approaches to zero (i.e., unmyelinated axon).

Let us take Lieberstein eqs. (8) and (9), introducing parameters  $\mu$  and  $\gamma$  characterizing the AP propagation velocity increase from saltatory conduction [4] and other relevant mechanisms. Note that in the book by Bressloff [4] which we have used as one of the sources of inspiration in regards to saltatory conduction the parameter  $D$  (14), modulates the signal dynamics across the membrane (related to  $\gamma$  here). However, the parameter  $\mu$  affects the quantity  $i_a$  which is the current along the axis of the axon. We can write the governing equations as:

$$\frac{\partial Z}{\partial t} + \Phi \cdot \left[ (1 + \gamma \cdot \mu) \cdot \frac{\partial i_a}{\partial x} + 2\pi a \cdot (\hat{g}_K n^4 (Z - Z_K) + \hat{g}_{Na} m^3 h (Z - Z_{Na}) + \hat{g}_l (Z - Z_l)) \right] = 0, \quad (15)$$

$$\frac{\partial i_a}{\partial t} + \frac{\pi a^2}{L} \cdot \left[ \frac{\partial Z}{\partial x} + r i_a \right] = 0, \quad (16)$$

$$\Phi = \frac{1}{C_a \pi a^2 + 2C_m \pi a}, \quad (17)$$

$$\mu = \frac{L_2}{L_1}. \quad (18)$$

In eq. (15) parameter  $\mu$  (18) ( $\mu$ -ratio) describes the average length of the myelinated section divided by the

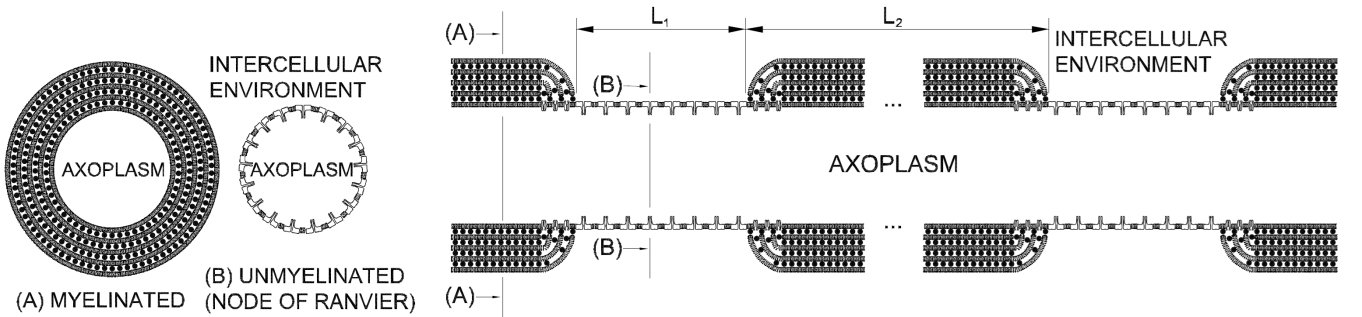


Figure 5: Simplified model geometry of the myelinated axon. Here  $L_1$  is the length of the node of Ranvier and  $L_2$  is the average effective length of the myelinated axon section.

average length of the node of Ranvier, i.e.,  $L_2/L_1$  in the Fig. 5 and parameter  $\gamma$  is a phenomenological coefficient which determines conduction velocity between adjacent nodes of Ranvier (generalized from eq. (14)). Here parameter  $\gamma$  includes myelin geometry perpendicular to the axon (related to  $g$ -ratio). As noted earlier, parameter  $\gamma$  is not taken here exactly like in (14) and is a generalized quantity. Here parameter  $\gamma$  is assumed to be between 0 and 1: if it is equal to 0, then the current can not propagate between the adjacent nodes (nodes of Ranvier are isolated from each other) and if it is equal to 1, then the myelinated sections are almost perfect conductors (i.e., very high propagation velocity) and adjacent nodes react to the changes in a given node almost immediately. Parameter  $\gamma$  could be considered like a generalized dimensionless relative

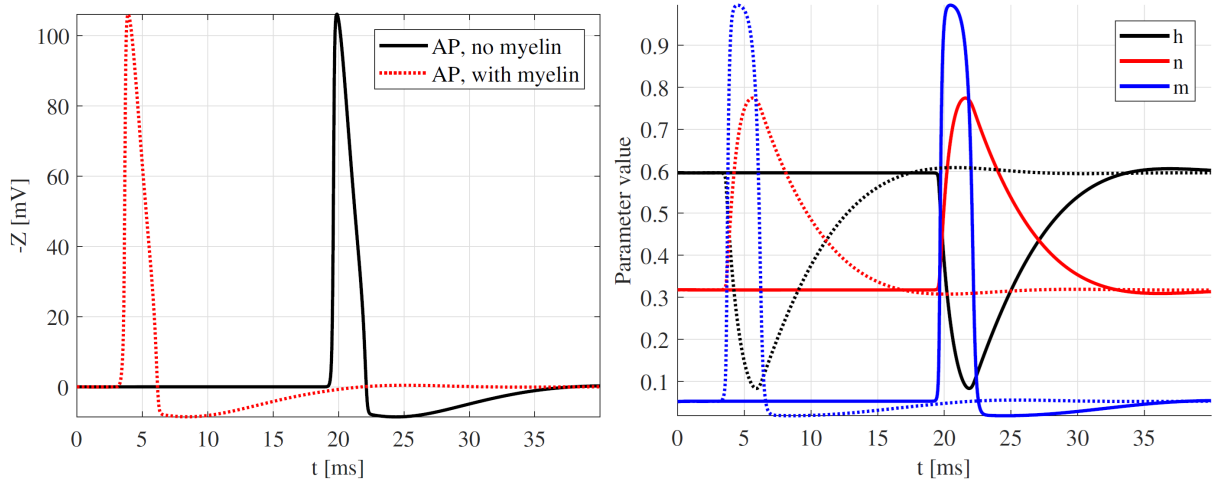


Figure 6: AP in time (left panel) and parameters  $n, m, h$  in time at  $n = 700$ . Initial spark is given at  $n = 1024$  at  $t = 1$  [ms], number of spatial nodes is  $n = 2048$ . Dotted lines – myelinated case, solid lines – unmyelinated case

velocity potentially containing all the physical effects (not only resistance but also diffusive, capacitive, inductance effects, the influence of cytoskeleton or even damage or pathological effects, etc) as it is chosen here. One should also stress that in the following example, we take  $\gamma = 1$  for the sake of simplicity, however, it would be logical that as the length of myelinated sections  $L_2$  increases then at some point the parameter  $\gamma$  would start to decrease. Using the same parameters as in the classical paper by Hodgkin and Huxley [19], a numerical example using parameter value  $\mu = 50$  (assuming  $1 \mu\text{m}$  nodes of Ranvier,  $50 \mu\text{m}$  length for myelinated sections and taking  $\gamma = 1$  for the numerical example) follows. Choosing  $\gamma = 1$  (which is an upper limit case) means that we are making here an assumption that saltatory conduction velocity is much faster than signal propagation velocity in an unmyelinated axon. We have to emphasize here that the “unit cell” we are modelling in the computational node contains both the node of Ranvier and the myelinated section adjacent to it, i.e., the parameters are a mix of “pure” Lieberstein model for unmyelinated axon and myelination effects like in [4].

One can note that in time (at a fixed spatial node, Fig. 6) the solutions look practically identical. However, it must be noted that in space the faster (in myelinated axon) AP is shaped significantly wider, as the dynamics of the ion channels are still the same as before, but as the wavefront propagates faster, its dominant wavelength in space is longer.

The AP propagation velocity as a function of the  $\mu$ -ratio  $\mu = L_2/L_1$  at a fixed axon radius ( $a = 1\mu\text{m}$ ,  $a = 4\mu\text{m}$ ,  $a = 8\mu\text{m}$ ,  $a = 16\mu\text{m}$ , and  $a = 32\mu\text{m}$ ) is depicted in Fig. 7. The case  $\mu = 0$  corresponds to an unmyelinated axon. It should be noted that here we are assuming that the thickness of the myelin (related to g-ratio, which is included through coefficient  $\gamma$  (14)) is the same even if  $\mu$ -ratio  $\mu$  is varied. The upper limit case ( $\gamma = 1$ ) for the conduction velocity is used. It should be noted that the dependence of the AP velocity on the axon radius is still there even in the myelinated case. The larger the radius of the axon, the faster the velocity of the AP increases as the  $\mu$ -ratio  $\mu = L_2/L_1$  is increasing.

## 4.2 On AP energy in myelinated axon

As a first rough estimate for the energy of AP, we can take it as the energy contained in an electric field on a capacitor. Taking the simplified axon geometry as a cylinder with a charge difference across the membrane one can make a naive simplification that the capacitance of such a cylinder segment is the same as a classical plate capacitor

$$C = \varepsilon_0 \kappa \frac{A}{d}, \quad (19)$$

where  $\varepsilon_0 = 8.85418782 \cdot 10^{12} \left[\frac{F}{m}\right]$  is the electric constant or vacuum permittivity,  $\kappa$  is the dielectric constant (roughly 7 for lipid bi-layer),  $A$  is area (for cylinder wall  $A = 2\pi ah$  where  $a$  is the radius and  $h$  is the length) and  $d$  is the thickness of insulating layer between the plates. As an example, for a rough estimate let us

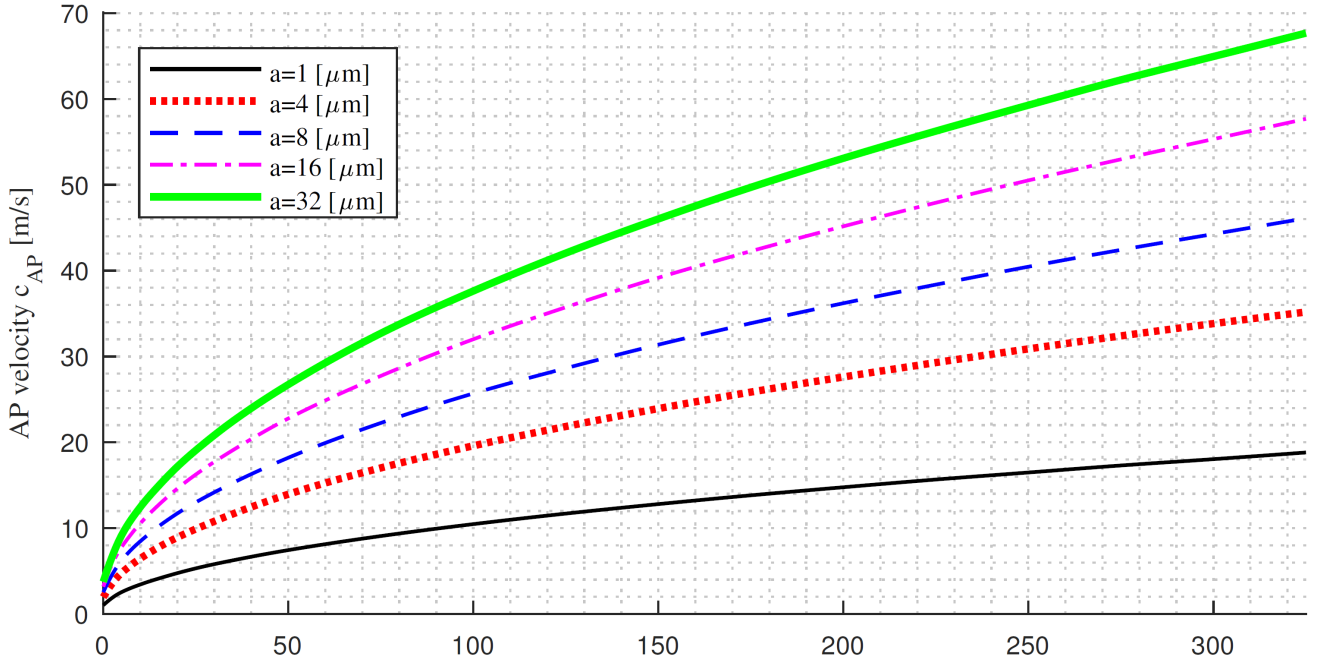


Table 2: AP velocity  $c_{AP}$  against  $\mu$ -ratio.

$\mu = L_2/L_1$ :	0	25	50	75	100	125	150	175	200	225	250	275	300	325
$a = 1[\mu m]$	1	5.3	7.5	9	10.5	11.7	12.8	13.8	14.8	15.7	16.5	17.3	18	18.8
$a = 4[\mu m]$	1.9	9.9	13.9	17	19.6	21.8	23.9	25.9	27.6	29.3	30.9	32.4	33.8	35.2
$a = 8[\mu m]$	2.5	13	18.2	22.3	25.7	28.6	31.4	33.9	36.2	38.4	40.5	42.4	44.3	46.1
$a = 16[\mu m]$	3.2	16.3	22.8	27.8	32	35.8	39.2	42.3	45.2	47.9	50.5	53	55.3	57.7
$a = 32[\mu m]$	3.8	19	26.7	32.7	37.6	42	46	49.7	53	56.3	59.3	62.2	65	67.7

Figure 7: Action potential propagation velocity as a function of  $\mu$ -ratio  $\mu = L_2/L_1$  in the modified Lieberstein model at fixed axon radius of  $a = 1\mu m$ ,  $a = 4\mu m$ ,  $a = 8\mu m$ ,  $a = 16\mu m$ , and  $a = 32\mu m$ . The table in the bottom panel contains the values of AP velocity  $c_{AP}$  [m/s].

take  $a = 1[\mu m]$ ,  $h = 1[cm]$  and  $d = 4[nm]$ . Inserting the noted values into the (19), we get capacitance of roughly  $10[nF]$  (per  $cm$  of axon).

The energy stored in the electric field in a charged parallel plate capacitor can be expressed as

$$E_C = \frac{1}{2}CZ^2, \quad (20)$$

where  $C$  is capacitance and  $Z$  is potential difference. Assuming  $\Delta Z = 100mV$ , we get a rough estimate as  $0.5 \cdot 10^{-11}J$  per  $cm$ .

This is a rough estimate for an unmyelinated axon (i.e., the node of Ranvier) because any geometry variations or possible changes of the dielectric constant during AP generation are neglected. Also, it must be noted that the electric field is quite significant in the unmyelinated sections (approximately  $100[mV]$  potential difference across only roughly  $4[nm]$  distance yields an electric field of  $2.5 \cdot 10^7 [\frac{V}{m}]$ .

Now if we add into our consideration the myelination it seems reasonable to assume that energy must be conserved, i.e., when the AP signal is “jumping” between the nodes of Ranvier the energy of the pulse is roughly the same  $0.5 \cdot 10^{-11}[J]$  per  $cm$  as we estimated for the node of Ranvier where the main difference is that the thickness of the insulating layer is much larger. For example, let us take  $d = 0.5[\mu m]$ . In such a case the capacitance estimate drops to roughly  $8[pF]$  per  $cm$  if all other parameters remain the same and the average electric field in the insulating layer drops to about  $2 \cdot 10^5 [\frac{V}{m}]$  for a  $500[nm]$  myelination thickness.

However, one should note that in the myelinated case, the signal is substantially faster and as a result the AP is spread over a significantly longer section of the axon in the myelinated case. One can argue that if considering the “total” AP signal energy (over its whole duration, at a fixed spatial point or at a fixed time over its whole spatial distribution) it could make more sense to consider the  $Z^2$  integral. Considering this

we can combine eqs. (19) and (20) replacing the plain  $Z^2$  with the integral over half-space can write

$$E_C = \frac{1}{2} \left[ \varepsilon_0 \kappa \frac{A}{d} \right] \int_0^{x/2} Z^2 dx, \quad \text{or} \quad E_C = \frac{1}{2} \left[ \varepsilon_0 \kappa \frac{A}{d} \right] \int_0^t Z^2 dt, \quad (21)$$

as a rough estimate of the total energy of the electric field for AP in space or in time, respectively. Note that we have assumed here that only a single AP pulse exists in the half-space or within the given timeframe for eq. (21).

On the other hand, considering only the question of capacitor energy is only one aspect of the AP energy. One could ask how the inclusion of inductivity  $L$  affects the calculation of AP energy? As a first approximation, one could be tempted to consider the energy in transmission line (1), (2) including inductivity (see Fig. 8 for a scheme of a unit cell) as opposed to just capacitor energy as it is usually done in literature for HH models. However, authors of the present paper remain somewhat sceptical towards such an approach as it is not entirely clear if considering magnetic field energy on such a small scale in the electrically conductive environment inside an axon would yield a reasonable estimate, even if we insist on including the noted inductivity. After all, the model proposed here does not include the influence of the cytoskeleton explicitly (although its influence on the AP propagation is taken into account indirectly through parameter  $\gamma$ ).

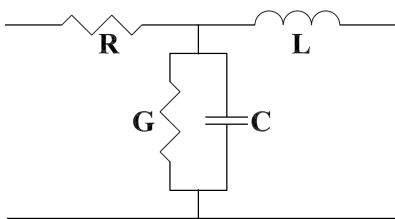


Figure 8: Unit cell of a transmission line [15, 18]. Resistance  $R$  [ $\frac{\Omega}{m}$ ], inductivity  $L$  [ $H \cdot m$ ], capacitance  $C$  [ $\frac{F}{m}$ ], conductance  $G$  [ $\frac{\Uparrow}{m}$ ].

Another possibility is to approach the question of the energy of AP from the perspective of power. It is known that power is  $P = I \cdot Z$ , where  $I$  is the current in a circuit and  $Z$  is the potential difference. Considering the power we could separate it into two components, first, across the membrane at a fixed spatial point  $P_m = I_m \cdot Z$  where  $I_m$  is the current across the membrane (taken similar to the HH model here) and  $Z$  is the AP amplitude at the given spatial point at given time (about  $100mV$  at the peak) and second, along the axon at the fixed time  $P_a = i_a \cdot Z_x$  where  $i_a$  is current along the axis of the axon and  $Z_x$  is the potential gradient along the axis of the axon.

## 5 Discussion and summary

We started with the elementary form of Maxwell equations (1), (2) and drawing inspiration from the classical HH paper [19] used the total membrane current density (6) to derive the model equations for unmyelinated axon similar to the Lieberstein model [25]. While Lieberstein opted to go a step further by moving into a moving frame of reference we opted to stay with the form which is closer to the Maxwell equations for a transmission line eqs. (8), (9) and used the work of Lieberstein as a source of inspiration for handling the question of inductance  $L$  in the context of signal propagation along the nerve axon. Using the parameters from the literature we investigated briefly the solutions of the noted model for the unmyelinated axon and demonstrated that the behaviour of the solutions is in the physiologically plausible range and the key characteristics of the nervous signalling are fulfilled. These are: (i) the annihilation of AP signals during a head-on collision, (ii) the existence of activation threshold, and (iii) the refraction period after signal passing. In the parameter range considered, we observe the AP signal propagation velocity  $c_{AP}$  from  $0.5$  [ $m/s$ ] up to about  $4.4$  [ $m/s$ ] for the unmyelinated axon. The key difference between the classical HH model and the Lieberstein-inspired model used here is that the mechanism for signal propagation along the axon emerges more ‘naturally’ as a consequence of opting to keep the inductivity  $L$ . While, indeed, there exist variations of the classical HH model which support AP signal propagation where the model is written in the form of PDE instead of the usual ODE form (which describes signal evolution in time at a fixed spatial point). In these, normally, the potential-gradient-type member responsible for propagating the signal along the axon is not

as clearly defined from a physical first-principles viewpoint (usually some kind of abstracted diffusion-type process is used). This is essential later in the paper for the purpose of clearer physical interpretation as we make use of the model based on the elementary form of Maxwell equations which is further modified to include the influence of myelination on the signal propagating along the axon.

We briefly explained the saltatory conduction mechanism hypothesis as we prepared to modify the governing equations to take into account the effect of myelination on the propagation of the AP along the axon. The model (8), (9) based on Maxwell equations for a transmission line is then modified to include the influence of myelination. In addition to the g-ratio normally considered in the earlier studies (taken into account indirectly through coefficient  $\gamma$ ) which takes into account the myelination geometry perpendicular to the axon we introduce the so-called “myelination-ratio” or  $\mu$ -ratio which describes the influence of myelin distribution on the signal propagation in the direction of the axis of the axon. The numerical example (see Fig. 7), using parameters from the literature, demonstrates physiologically plausible behaviour for the model. The model is reduced to the initial model if the length of the myelinated sections along the axon is taken as zero and under the considered parameter combinations we can observe the AP propagation velocities up to 67.7 [m/s] (the signal propagation velocity range for myelinated axons is given as roughly 10 to 100 [m/s] in the earlier studies).

It is important to emphasize that the proposed continuum-based model is philosophically similar to how the transmission line equations are composed. The ‘unit-cell’ in the context of the myelinated axon in the model is composed of the node of Ranvier and the myelinated section next to it. This is opposed to the alternative approach which is also relatively popular in the literature where the classical HH model is used in the nodes of Ranvier while myelinated sections are handled separately either through some numerical scheme or by an alternative model coupled with the HH model in the node of Ranvier through some mechanism. Having a relatively simple pair of PDEs which are connected to the fundamental principles in physics (i.e., Maxwell equations for anything involving the movement of charges in an environment) could be considered superior to investigating causal connections and making predictions than something that is not as clearly connected to the first principles of physics.

Finally, we briefly discuss the question of the energy of the AP pulse in both myelinated and unmyelinated axons, making an argument that while the normally used capacitor-energy-based energy estimate is a reasonable starting point, something more could be needed. Speculating that perhaps instead of considering capacitor energy as the energy of an AP signal it could be better to consider the power of the signal (either in space, at a fixed time or in time, at a fixed spatial point).

## Acknowledgement

This research was supported by the Estonian Research Council (PRG 1227). Jüri Engelbrecht acknowledges the support from the Estonian Academy of Sciences.

## References

- [1] I. L. Arancibia-Carcamo and D. Attwell. The node of Ranvier in CNS pathology. *Acta Neuropathologica*, 128(2):161–175, 2014.
- [2] I. L. Arancibia-Cárcamo, M. C. Ford, L. Cossell, K. Ishida, K. Tohyama, and D. Attwell. Node of Ranvier length as a potential regulator of myelinated axon conduction speed. *eLife*, 6:1–15, 2017.
- [3] P. J. Basser. Scaling laws for myelinated axons derived from an electronic core-conductor model. *Journal of Integrative Neuroscience*, 03(02):227–244, 2004.
- [4] P. C. Bressloff. *Waves in Neural Media*. Lecture Notes on Mathematical Modelling in the Life Sciences. Springer New York, New York, NY, 2014.
- [5] H. Chen, D. Garcia-Gonzalez, and A. Jérusalem. Computational model of the mechanoelectrophysiological coupling in axons with application to neuromodulation. *Physical Review E*, 99(3):032406, 2019.

- [6] D. Debanne, E. Campanac, A. Bialowas, E. Carlier, and G. Alcaraz. Axon physiology. *Physiological Reviews*, 91(2):555–602, 2011.
- [7] D. A. Doyle, J. M. Cabral, R. A. Pfuetzner, A. Kuo, J. M. Gulbis, S. L. Cohen, B. T. Chait, and R. MacKinnon. The structure of the potassium channel: Molecular basis of K<sup>+</sup> conduction and selectivity. *Science*, 280(5360):69–77, 1998.
- [8] A. El Hady and B. B. Machta. Mechanical surface waves accompany action potential propagation. *Nature Communications*, 6:6697, 2015.
- [9] J. Engelbrecht. On theory of pulse transmission in a nerve fibre. *Proceedings of the Royal Society A: Mathematical, Physical and Engineering Sciences*, 375(1761):195–209, 1981.
- [10] J. Engelbrecht, K. Tamm, and T. Peets. *Modelling of Complex Signals in Nerves*. Springer International Publishing, Cham, 2021.
- [11] J. Engelbrecht, K. Tamm, and T. Peets. Axons’ Signals. In A. Costa and E. Villalba, editors, *Horizons in Neuroscience Research. Volume 49*, chapter 3, page 223. Nova Science Publishers, Inc., New York, NY, 2023.
- [12] R. D. Fields. Myelin - More than insulation. *Science*, 344(6181):264–266, 2014.
- [13] R. Fitzhugh. Computation of Impulse Initiation and Saltatory Conduction in a Myelinated Nerve Fiber. *Biophysical Journal*, 2(1):11–21, 1962.
- [14] B. Frankenhaeuser and A. F. Huxley. The action potential in the myelinated nerve fibre of *Xenopus laevis* as computed on the basis of voltage clamp data. *The Journal of Physiology*, 171(2):302–315, 1964.
- [15] A. Fukasawa. Electrophysical Modelling and Analysis of Axon in Neurons. 1:66–71, 2016.
- [16] L. Goldman and J. S. Albus. Computation of Impulse Conduction in Myelinated Fibers; Theoretical Basis of the Velocity-Diameter Relation. *Biophysical Journal*, 8(5):596–607, 1968.
- [17] J. Hanig and G. Negi. *Myelin: Structure, function, pathology, and targeted therapeutics*. Elsevier Inc., second edition, 2018.
- [18] W. Hayt and J. Buck. *Engineering Electromagnetics*. McGraw-Hill, 2012.
- [19] A. L. Hodgkin and A. F. Huxley. A quantitative description of membrane current and its application to conduction and excitation in nerve. *The Journal of Physiology*, 117(4):500–544, 1952.
- [20] A. L. Hodgkin and B. Katz. The effect of temperature on the electrical activity of the giant axon of the squid. *The Journal of Physiology*, 109(1-2):240–249, 1949.
- [21] A. F. Huxley and R. Stämpfli. Evidence for saltatory conduction in peripheral myelinated nerve fibres. *The Journal of physiology*, 108(3):315–39, 1949.
- [22] K. Iwasa and I. Tasaki. Mechanical changes in squid giant axons associated with production of action potentials. *Topics in Catalysis*, 95(3):1328–1331, 1980.
- [23] K. H. Kang and M. F. Schneider. Nonlinear pulses at the interface and its relation to state and temperature. *The European Physical Journal E*, 43(2):8, 2020.
- [24] S. Kaplan and D. Trujillo. Numerical studies of the partial differential equations governing nerve impulse conduction: the effect of lieberstein’s inductance term. *Mathematical Biosciences*, 7(3-4):379–404, 1970.
- [25] H. Lieberstein. On the Hodgkin-Huxley partial differential equation. *Mathematical Biosciences*, 1(1):45–69, 1967.
- [26] R. S. Lillie. FACTORS AFFECTING TRANSMISSION AND RECOVERY IN THE PASSIVE IRON NERVE MODEL. *Journal of General Physiology*, 7(4):473–507, 1925.

- [27] H. Lodish, A. Berk, P. Matsudaira, C. A. Kaiser, M. Krieger, and M. P. Scott. Transport of Ions and Small Molecules Across Cell Membranes. *Molecular Cell Biology*, pages 245–300, 2004.
- [28] P. Lucht. *Transmission Lines and Maxwell’s Equations*. Rimrock Digital Technology, Salt Lake City, 2014.
- [29] D. Massey, N. Cunniffe, and I. Noorani. *Carpenter’s Neurophysiology*. CRC Press, Boca Raton, 2022.
- [30] G. V. Michailov, M. Sereda, B. Brinkmann, T. Fischer, B. Haug, C. Birchmeier, L. Role, C. Lai, M. Schwab, and K.-A. Nave. Axonal Neuregulin-1 Regulates Myelin Sheath Thickness. *Science*, 304(5671):700–703, 2004.
- [31] A. Raasakka, S. Ruskamo, J. Kowal, H. Han, A. Baumann, M. Myllykoski, A. Fasano, R. Rossano, P. Riccio, J. Bürck, A. S. Ulrich, H. Stahlberg, and P. Kursula. Molecular structure and function of myelin protein P0 in membrane stacking. *Scientific Reports*, 9(1):1–15, 2019.
- [32] W. A. H. Rushton. A theory of the effects of fibre size in medullated nerve. *The Journal of Physiology*, 115(1):101–122, 1951.
- [33] F. K. Sanders. The thickness of the myelin sheaths of normal and regenerating peripheral nerve fibres. *Proceedings of the Royal Society of London. Series B - Biological Sciences*, 135(880):323–357, 1948.
- [34] H. Schmidt and T. R. Knösche. Action potential propagation and synchronisation in myelinated axons. *PLOS Computational Biology*, 15(10):e1007004, 2019.
- [35] A. Sula, J. Booker, L. C. Ng, C. E. Naylor, P. G. Decaen, and B. A. Wallace. The complete structure of an activated open sodium channel. *Nature Communications*, 8:2–10, 2017.
- [36] C. Sun, J. D. Achenbach, and G. Herrmann. Continuum Theory for a Laminated Medium. *Journal of Applied Mechanics*, 35(3):467, 1968.
- [37] K. Tamm, T. Peets, and J. Engelbrecht. Mechanical waves in myelinated axon wall. (0123456789), 2021.
- [38] I. Tasaki. A macromolecular approach to excitation phenomena: mechanical and thermal changes in nerve during excitation. *Physiological chemistry and physics and medical NMR*, 20(4):251–268, 1988.
- [39] I. Tasaki and P. M. Byrne. Heat production associated with a propagated impulse in Bullfrog myelinated nerve fibers. *The Japanese Journal of Physiology*, 42(5):805–813, 1992.
- [40] I. Tasaki and M. Fujita. Action currents of single nerve fibers as modified by temperature changes. *Journal of Neurophysiology*, 11(4):311–315, 1948.
- [41] I. Tasaki, K. Kusano, and P. M. Byrne. Rapid mechanical and thermal changes in the garfish olfactory nerve associated with a propagated impulse. *Biophysical Journal*, 55(6):1033–1040, 1989.
- [42] S. Terakawa. Potential-dependent variations of the intracellular pressure in the intracellularly perfused squid giant axon. *The Journal of Physiology*, 369(1):229–248, 1985.
- [43] G. S. Tomassy, D. R. Berger, H.-H. Chen, N. Kasthuri, K. J. Hayworth, A. Vercelli, H. S. Seung, J. W. Lichtman, and P. Arlotta. Distinct Profiles of Myelin Distribution Along Single Axons of Pyramidal Neurons in the Neocortex. *Science*, 344(6181):319–324, 2014.
- [44] H. Wang, J. Wang, G. Cai, Y. Liu, Y. Qu, and T. Wu. A Physical Perspective to the Inductive Function of Myelin-A Missing Piece of Neuroscience. *Frontiers in Neural Circuits*, 14(January):1–23, 2021.
- [45] G. Whitham. *Linear and Nonlinear Waves*. Wiley-Interscience, New York, 1974.
- [46] Y. Yang, X.-W. Liu, H. Wang, H. Yu, Y. Guan, S. Wang, and N. Tao. Imaging Action Potential in Single Mammalian Neurons by Tracking the Accompanying Sub-Nanometer Mechanical Motion. *ACS Nano*, 12(5):4186–4193, 2018.
- [47] R. G. Young, A. M. Castelfranco, and D. K. Hartline. The ”Lillie Transition”: models of the onset of saltatory conduction in myelinating axons. *Journal of Computational Neuroscience*, 34(3):533–546, 2013.